Combustion-assisted solar gasification of biomass particles in a high temperature conical jet spouted bed reactor

Houssame Boujjat, Sylvain Rodat, Srirat Chuayboon, Stéphane Abanades

Combustion-assisted solar gasification of biomass particles in a high temperature conical jet spouted bed reactor

Cite as: AIP Conference Proceedings **2303**, 170002 (2020); https://doi.org/10.1063/5.0028585
Published Online: 11 December 2020

Houssame Boujjat, Sylvain Rodat, Srirat Chuayboon, and Stéphane Abanades

Combustion-assisted Solar Gasification of Biomass Particles in a High Temperature Conical Jet Spouted Bed Reactor

Houssame Boujjat[1,2], Sylvain Rodat[1,2], Srirat Chuayboon[3], Stéphane Abanades[3,*]

[1] *Univ. Grenoble Alpes, INES, BP 332, 50 Avenue du Lac Leman, F-73375 Le-Bourget-du-lac, France*
[2] *CEA-LITEN Laboratory of Solar Systems and Thermodynamics (L2ST), F-38054 Grenoble, France*
[3] *Processes, Materials and Solar Energy Laboratory, PROMES-CNRS, 7 Rue du Four Solaire, 66120 Font-Romeu, France*

*Corresponding author: Stephane.Abanades@promes.cnrs.fr

Abstract. The combination of biomass and solar energy in a solar-driven thermochemical gasification process is of particular interest to convert solid carbonaceous materials to syngas, consisting chiefly of CO and H_2, thereby offering an efficient means of storing intermittent solar energy into carbon neutral solar fuels. The development of solar gasifiers suffers from the inherent issue of solar energy variability caused by cloud passages and shut off at night. The concept of hybrid solar/autothermal reactors is proposed to meet the requirement of continuous operation under fluctuating solar radiation. The hybrid reactor harvests the thermal energy from both solar heat (allothermal) and partial oxy-combustion of the feedstock (autothermal) if the solar resource is not high enough to reach the minimum temperature for the gasification reaction. In this work, for the first time a directly and indirectly irradiated hybrid reactor subjected to real concentrated solar flux was experimentally studied and modelled. Effects of O_2 injection on temperature distribution, gas production rates and LHV are discussed. In order to provide a better overview of the reactor thermal, chemical and hydrodynamic behavior, a 3D Computational Fluid dynamics (CFD) model was developed. Results in terms of temperature and velocity profiles, reactive particles trajectories inside the reaction chamber, syngas composition for the allothermal and hybrid model are provided. The study showed that process hybridization is relevant to control the reactor temperature although significantly impairing the syngas yield and quality.

INTRODUCTION

The significant interest and benefits of solar gasification raise the need to address the issue of intermittent solar energy to adapt to varying input power and to ensure continuous operation. Process hybridization through coupled solar heating and partial feedstock oxy-combustion appears to be an efficient and cost effective solution to compensate the variable nature of solar radiations. Current solar hybrid technologies can be classified into three different categories depending on the annually averaged consumed solar energy [1]: (i) Solar Aided Combustion Generation Systems use solar energy to cover at maximum 33% of their energy requirements, (ii) Balanced Solar-Combustion Generation Systems use between 33% to 66% of solar to meet their energy needs, (iii) Combustion Aided Solar Generation Systems, in which more than 66% of the system's total energy is provided by solar solely. To date solar hybrid reactor technologies utilize solar receivers to harvest the solar radiation and back up combustors to mitigate the fluctuations in the solar resource. This penalizes the thermal efficiency due to the use of heat exchangers and requires highly reliable and synchronized thermal systems. Alternatively, direct hybrid solar technologies allow to take advantage of both solar and combustion thermal energy in the same equipment; thus sharing both the supporting infrastructure and non-solar devices [2]. In addition to simplifying the interactions between the process subsystems, direct hybrids contribute clearly to the reduction of the plant capital cost. In solar allothermal gasification, cavity type solar reactors were extensively used to achieve the high gasification temperatures due to their low radiation heat losses [3]. These devices are characterized by an aperture that lets the concentrated solar power entering the cavity; moreover, they offer the possibility to exploit in-situ homogeneous and heterogeneous combustion reactions. Three operating modes

SolarPACES 2019
AIP Conf. Proc. 2303, 170002-1–170002-9; https://doi.org/10.1063/5.0028585
Published by AIP Publishing. 978-0-7354-4037-1/$30.00

are possible [4]. The allothermal mode is most appropriate when the available solar energy is sufficient to maintain the gasification temperature at or above fixed set-point value. The hybrid mode involves mixed solar and combustion to control the process temperature. The shift to the autothermal combustion-only mode (partial feedstock combustion) occurs gradually as the solar insolation decreases. Several experimental studies on allothermal solar gasification (solar heating only) have demonstrated the feasibility and efficiency of these processes [5-7]. However, very little research has been undertaken concerning mixed solar/combustion reactors. Most of the earlier works dealt with the simulation of hybrid solar gasification at a system scale based on equilibrium models [8-10]. These models have definitely shown the interest of hybridization to promote process integration. Experimental validation tests under direct real concentrated solar power and detailed 3D numerical simulations of solar hybrid gasification have never been performed. Muroyama et al. [11] studied an indirectly heated solar hybrid fluidized bed reactor for activated carbon gasification. In the continuity of these first results, we experimentally investigated a solar hybrid reactor that can operate in both direct and indirect heating modes. This work aims to study solar hybrid gasification of biomass in a novel lab scale reactor based on the principle of conical jet spouted beds. Solar-only and mixed solar-combustion experiments were carried out under real concentrated solar flux for both direct and indirect heating configurations. O2 injection aims to control the set point temperature of the reactor. The effects of process hybridization on the reactor throughput (syngas yield and on the gasifier performance) were investigated. A Computational Fluid Dynamics (CFD) model was also developed in order to get a better understanding of the conversion process and to provide insights into the reactor temperature distribution, fluid flow dynamics, and flame location inside the reaction zone. The model was used to analyze the thermal, chemical and hydrodynamic behavior of the reactor when operating in both allothermal and hybrid solar/autothermal mode. Model predictions were compared with experimental results.

EXPERIMENTAL SET UP

The studied 60° angle conical spouted bed cavity-type reactor is settled at the focus of a parabolic solar concentrator located at the 6th floor of the CNRS-PROMES building (Fig.1). The top of the metallic cavity is composed of an alumina cap with an aperture that lets the concentrated solar rays entering the cavity. A key feature of this reactor is a removable emitter plate that enables to operate with direct (no plate) or indirect (plate installed) solar irradiation. All along the experiments, a sun tracking heliostat was used to reflect the solar rays towards a parabolic mirror that in turn concentrates the radiations towards the reactor aperture.

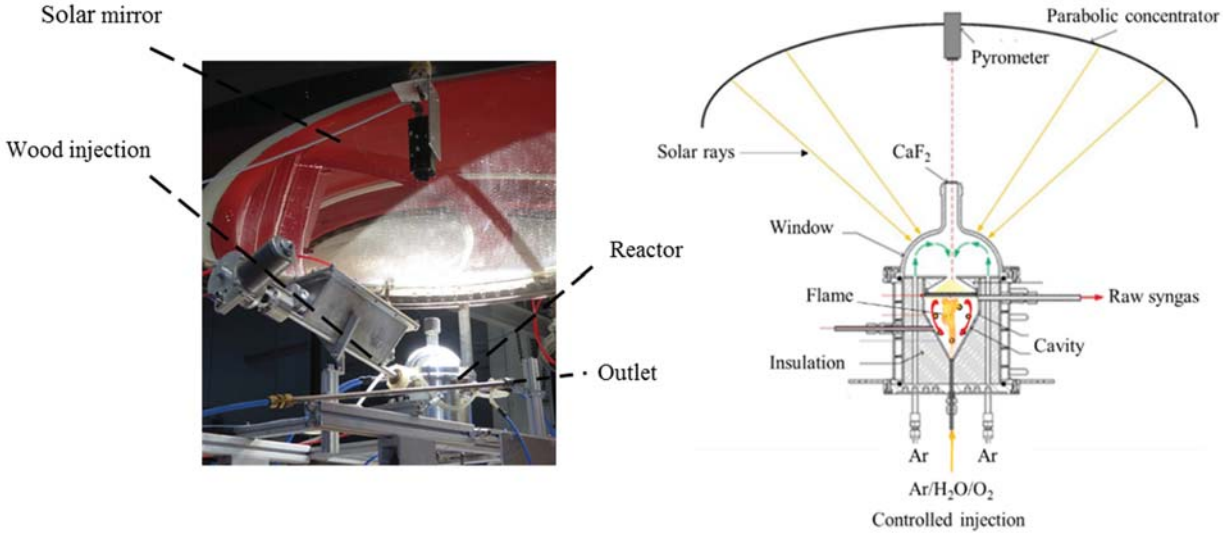

FIGURE 1. Reactor coupling with CNRS vertical-axis solar furnace and scheme of the hybrid solar/combustion spouted bed reactor at the focus of the solar concentrator

The biomass was first loaded in a hopper (1.15 L capacity) connected to a screw feeder for continuous particle injection in the reactor cavity at high temperatures. An Ar flow of 0.5 L/min was continuously injected in the hopper so that the hot gases from the cavity cannot interact with the reactive feedstock. Moreover, to prevent the reactor window from fouling and overheating, a protective Ar flow (2 NL/min) was constantly injected from the bottom to

sweep the window away and make sure that all the gases exit the reactor from the outlet. A gas jet composed of Ar and steam was injected from the bottom cavity via an alumina tube. The gas jet was composed of 0.2 NL/min of Ar and 200 mg/min of steam thus providing a slightly over-stoichiometric Steam-to-Biomass (S/B) ratio. The beech wood particles continuously fell into the conical cavity to get spouted cyclically by the entering high velocity oxidant and carrier gas. Biomass characteristics are summarized in Table 1. The outlet syngas was analyzed continuously using an on-line syngas analyzer (GEIT 3100) for measurement of the concentrations of the main species contained in the syngas every 3s. These measurements were checked with a gas chromatograph equipped with two columns using Ar as carrier gas (micro GC, Varian CP4900). The GC especially provides more accurate data concerning light hydrocarbons (C_2H_2, C_2H_4 and C_2H_6). To measure the reactor temperature, B-type thermocouples were inserted inside the conical part of the cavity (T1 at the cavity center and T3 near the bottom of the cavity in the conical region) and at the external cavity surface (T2). Their tips were protected from the reacting gases with an alumina shielding tube. A solar-blind pyrometer was also used to measure the temperature inside the cavity (direct heating) or at the surface of the emitter plate (indirect heating). Moreover, the direct normal irradiance (DNI) was measured all along the experiments by a pyrheliometer every 0.8s. To verify that the reactor was maintained at slightly above atmospheric pressure, three pressure measurements were set in the window area (P1), cavity (P2), and hopper (P3). The bottom inlet gas flow rate (gaseous reactants consisting of $Ar/H_2O/O_2$ mixture) and pressure drop are controlled such that the resulting high-velocity jet causes a stream of particles to rise rapidly in a hollowed central core, then to revert to the annular region between the central spout and the cavity walls. The vigorous cyclic flow of the particles in the conical cavity allows their maximum exposure to solar radiations while the solid residence time is increased.

TABLE 1. Biomass characteristics

	C (wt.%)	H (wt.%)	O (wt.%)	N (wt.%)	S (wt.%)	Ash (wt.%)	Moisture (wt.%)	Density (kg/m^3)	Heat capacity (J/kg.°C)
Beech wood	48.3	6.7	44.4	0.1	<0.1%	0.46	8	650	1500

EXPERIMENTAL INVESTIGATION

The objective here is to study experimentally for the first time the ability of hybridization in controlling the reaction temperature when operating the reactor in both directly and indirectly heating configurations. Experiments were carried out under stable solar conditions with a DNI that varied from 938 to 975 W/m² for Run#1 (indirect heating mode) and from 885 to 911 W/m² for Run#2 (direct heating mode). The nominal reactor temperature (TC3) was the same for the two runs fixed at 1300°C (at steady state). The operating conditions for the two runs are recapped in Table 2. To study the transient behavior of the reactor, and demonstrate its adaptability and flexibility for hybrid operation, O_2 was injected with the spout gases after a period of steady state solar-only steam gasification, as shown in Figure 2.

TABLE 2. Operating conditions for Run#1 (Indirect heating) and Run#2 (Direct heating)

	Run# 1		Run# 2	
$m_{feedstock}$	50g		50g	
Operating mode	Allothermal	Hybrid	Allothermal	Hybrid
$F_{biomass}$	1.2 g/min	1.4 g/min	1.2 g/min	1.4 g/min
F_{steam}	0.2 g/min	0.2 g/min	0.2 g/min	0.2 g/min
F_{oxygen}	0 NL/min	0.25 Nl/min	0 NL/min	0.25 Nl/min
$(B_{dry}/O_2)/(B_{dry}/O_2)_{st}$	-	4.95	-	4.95

Fig.2a shows the measurements of outlet gas production rate evolution with the on-line syngas analyzer (continuous lines) and the GC analysis (dots). Both measurements matched very well, thus demonstrating reliability of gas analysis. Fig.2b shows the measured DNI (W/m²) and solar power input (W). The solar power input was controlled by partially closing a trapdoor below the reactor frame to stabilize the reactor temperature. The observed small instabilities in Fig.2a in the gas production rates are due to fluctuating feeding rate because the screw feeder outlet cannot be directly inserted in the hot zone of the reactor, thus the biomass particles are pushed by preceding particles and fall into the cavity in the form of small parcels by gravity. Complete injection of the whole biomass feedstock was achieved with no remaining char in the cavity at the end of the two runs.

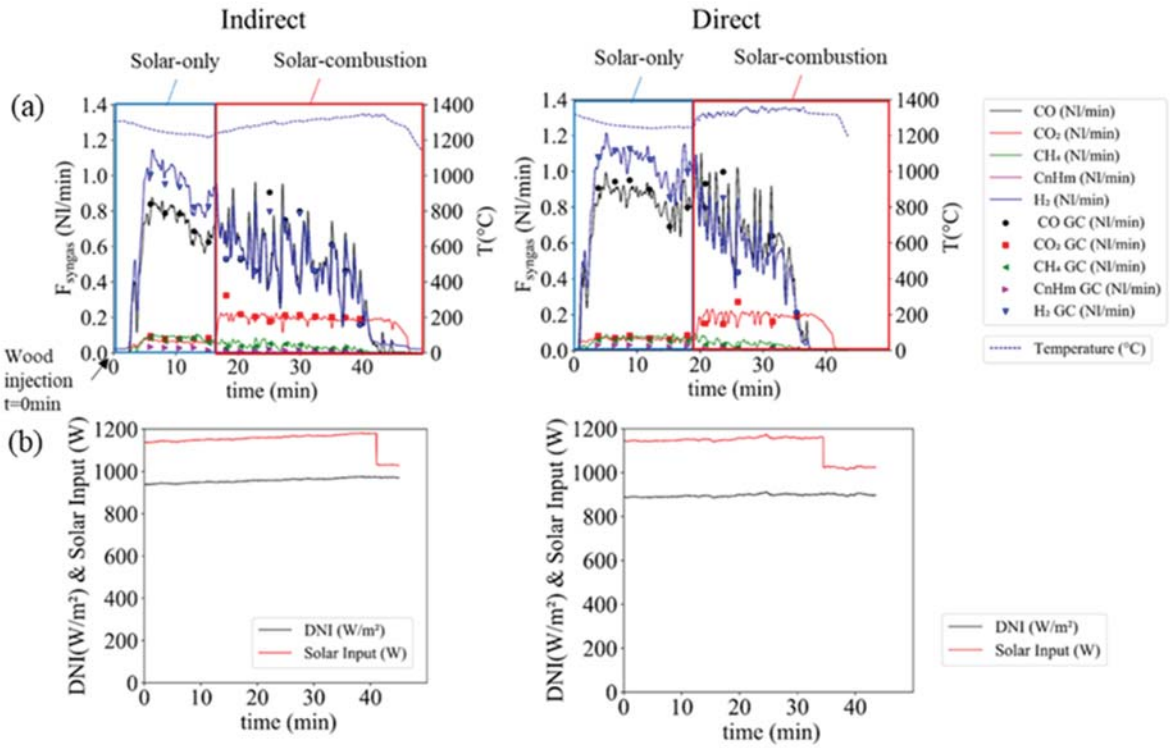

FIGURE 2. (a)- Syngas production rate and reactor temperature (TC3) as function of time: allothermal mode (1.2 g/min of wood, 200 mg/min of steam); hybrid mode (1.4 g/min of wood, 200 mg/min of steam, 0.25 Nl/min of oxygen) - Run#1 (Indirect) and Run#2 (Direct), (b)- Measured DNI (W/m2) and solar power input (W) as function of time

During the first 16 minutes (Run# 1) and 19 minutes (Run# 2) of allothermal operation, the produced syngas was composed of H_2 and CO mainly but temperature decreased because of the endothermal reactions (1307°C-1215°C in Run#1 and 1316°C-1245°C in Run# 2). Then, the wood feeding rate was increased from 1.2 to 1.4 g/min and the O_2 feeding rate was fixed to 0.25 Nl/min (to burn the excess amount of wood injected equal to 0.2 g/min). The biomass flow rate was adjusted to ensure that the same amount of wood particles is steam gasified before and after hybridization. An increase in the reactor temperature by 135°C (Run# 1) and 105°C (Run#2) was achieved thanks to internal exothermic heterogeneous and homogeneous oxycombustion reactions. This proves the possibility of maintaining the process temperature thanks to controlled oxy-combution. The reactor temperature as measured by TC3 (inside the cavity), TC2 (external cavity wall surface) and pyrometer (T_{pyro}) is also plotted in Fig.3. The pyrometer for the indirect heating mode measures the emitter plate temperature. For the direct heating mode, it points at the core of the conical cavity.

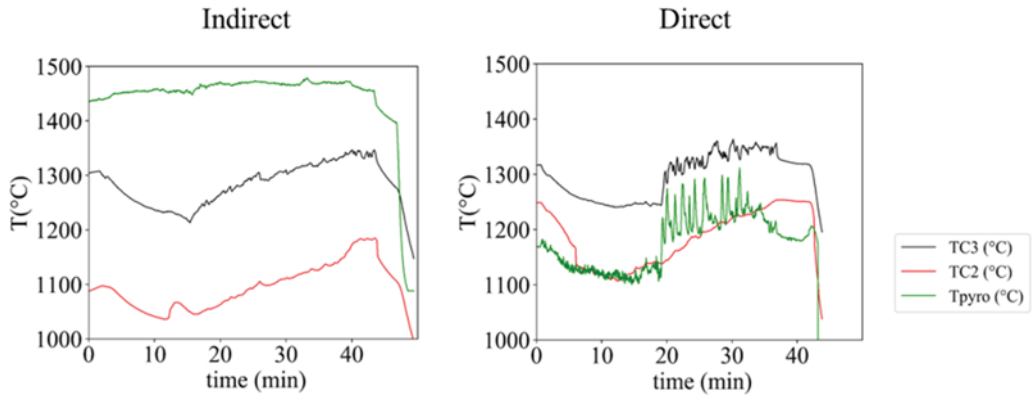

FIGURE 3. Reactor temperature measured by TC3, TC2 and pyrometer (T_{pyro}) in (°C)

It can be observed that TC2 indicates lower temperatures that are about 100°C to 150°C below TC3 as a result of internal thermal resistance of the metallic cavity wall. The plate temperature seems to be only slightly affected by the oxygen injection according to pyrometer measurements. In contrast, T_{pyro} shows for the direct heating mode a sharp increase in temperature and strong fluctuations. The latter are due to optical disturbances caused by the spouted char particles as well as by the injected raw (unreacted) biomass particles that fall by gravity to the bottom of the cone in the form of small parcels. These particles are subjected to temperatures variation when being spouted, which is clearly evidenced by the pyrometer measurements.

The increase in cavity temperature after O_2 injection was accompanied by an almost instantaneous decline of H_2 and CO production rates and a strong increase of CO_2 due to combustion. H_2 and CO_2 are found to be the most impacted gases in the mixture. This affects the syngas quality (H_2:CO ratio) and the syngas heating value (LHV). Fig.4 shows the time evolution of the H_2:CO and LHV before and after O_2 injection for the indirectly and directly solar heated reactor.

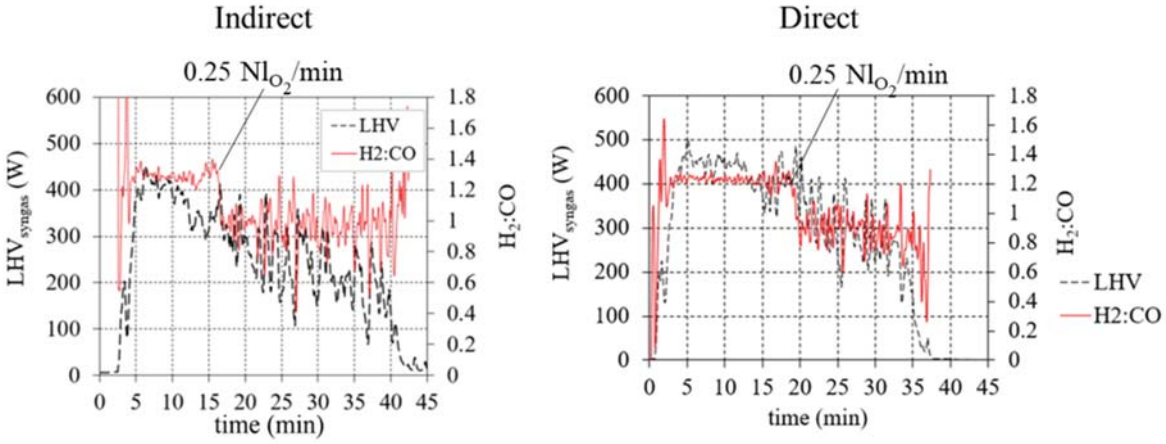

FIGURE 4. LHV and H_2:CO ratio as a function of time

It can be seen that the H_2:CO ratio declined from around 1.2 for the two modes to reach values approaching 0.9 (drop of 24%) after hybridization. The syngas thermal energy content also decreased significantly from 355 W for Run#1 and 430 W for Run#2 to 236 W and 301 W, respectively. Globally, the two heating modes showed very similar behavior, with a slightly higher gas production rates for the direct configuration especially during the allothermal phase of the experiments.

To get insights into the biomass thermochemical conversion inside the directly solar-radiated conical cavity. A 3D numerical model that takes into account both gas and particulate phase flows, radiation, energy, mass and momentum transfer coupled with chemical reactions (both pyro-gasification and combustion) was developed. The obtained results are discussed in the following section of this paper.

NUMERICAL SIMULATION

Model Development

The transport equations of momentum, mass, energy and radiation intensity (Discrete Ordinates model) were solved in 3D. Biomass particles are injected and tracked using the DPM (Euler-Lagrange) approach. The particulate phase exchanges heat, mass and momentum with the outer fluid phase environment. The particles are assumed spherical with a uniform temperature (intraparticle gradients not taken into account). Biomass decomposition (pyrolysis) follows the following scheme:

$$\text{Biomass} \rightarrow 2.77CO + 2.71H_2 + 0.35CO_2 + 0.45CH_4 + 0.44H_2O + 0.32C_6H_5OH_{(g)} + 0.52C_{(s)} \quad (1)$$

The kinetic of the pyrolysis reaction (rp) follows a first order Arrhenius law with $E_{a,pyrolysis}=7x10^7$ J/mol and Apyrolysis=$7.4x10^3$/s taken from the work of Chen [12] and Billaud et al. [13]. The pyrolysis coefficients of equation (1) were taken from the work of Septien et al. [14] who studied fast pyrolysis under inert atmosphere of millimetric beech wood particles at 800°C. This corresponds to the operating conditions for pyrolysis in the current study. The produced char (C(s)) reacts with steam and oxygen. The random pore model was used in this study for steam gasification. In this model, the gasification rate is calculated by equation (2).

$$r_g = \frac{dm_{char}}{dt} = -f(X).p_{H_2O}^N.\left(A_g e^{-E_g/RT_p}\right).m^{0,c} \quad (2)$$

$$X = 1 - \frac{m_{char}}{m_{char,o}} \quad (3)$$

$$f(X) = (1-X).\sqrt{1-\Psi.ln\,(1-X)} \quad (4)$$

The kinetic parameters used here are the same as the ones used by Septien et al. [14] for studying beech wood gasification in a Drop Tube Reactor (DTR) between 1000°C and 1400°C. In fact, Ψ was taken equal to 1 which is in the range of the values reported in the literature [15]. The activation energy Ea,g=149 kJ/mol, the frequency factor A_g=217893 $s^{-1}bar^{-0.7}$ and the order related to the oxidant N = 0.7 were determined, which also corresponds to the reported data [16]. The char oxy-combustion rate law used here includes the effects of both diffusion and kinetic rates (equation (5)):

$$r_c = \frac{dm_{char}}{dt} = A_{fuel}.Y_c.R_{KIN}(P_{O_2} - (r_c/D_0))^{0.65} \quad (5)$$

$$R_{KIN} = A_c e^{-E_c/RT_p} \quad (6)$$

$$D_0 = \frac{C(T_p+T)^{0.75}}{2d_p} \quad (7)$$

C is the diffusion rate constant, in most cases this coefficient is set to 5.10^{-12} $s/K^{0.75}$. This value can be deduced assuming that the rate of diffusion of the oxidant to the surface of the particle is in equilibrium with the rate of consumption by reaction at the surface. The global chemical reaction kinetics of gas and solid phase combustion reactions are the same as those used by Nakod [17] for modelling an oxy-fired entrained flow gasifier.

The particle size distribution of the studied biomass feedstock was characterized with a Camsizer XT (Retsch Company) by dynamic image analysis. The Probability Density Function (PDF) and the Cumulative Density Function (CDF) were modeled by a Rosin-Rammler distribution. The PDF parameters were determined so as to best fit the experimentally measured data.

The inlet gases are assumed to enter the reactor at 25°C. The reactor external borders are water-cooled and maintained at 25°C. The top surface of the reactor exchanges radiation with an external black body at 25°C ($Q_{Loss}=A.\varepsilon.\sigma(T^4-T^4_{ex})$). The radiative source representing the incoming concentrated solar power is a semi-transparent surface allowing reradiation outside of the reactor. On a geometrical point of view, the boundary condition for the radiative source is a circle arc subtending a 120° angle (semi-transparent wall), thus accurately representing the way the concentrated solar flux enters the reactor. The irradiation is specified in terms of a constant incident radiant heat flux (W/m^2) and is assumed specular.

Simulation Results

To visualize the effects of O_2 injection on the temperature field inside the cavity, two orthogonal cross sections of the reactor were plotted in Fig.5.

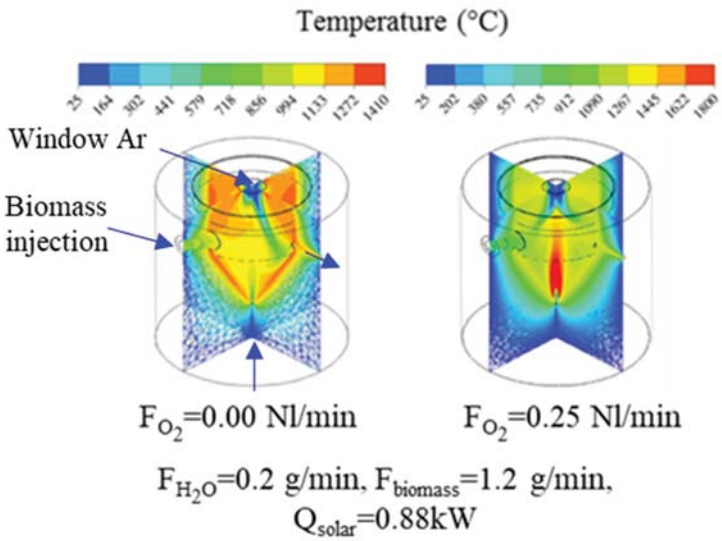

FIGURE 5. Temperature contour inside the reactor on two perpendicular vertical planes

It can be seen that for the allothermal operation (F_{O2}=0.00 Nl/min), the bottom inlet gases rapidly reach higher temperatures approaching 1050°C in the fluid phase. Moreover, the temperature appears to be homogeneously distributed inside the cavity and the cavity walls. A temperature gradient between the gas phase and cavity walls can however be observed. From the allothermal simulation, a flow rate of oxygen F_{O2}=0.25 Nl/min and an addition of 0.2 g/min of wood were computed for the hybrid operation simulation. It appears from the simulation that the central spout region reaches very high temperatures (~ 1800°C at central spout) while the annular zone is less affected by the O_2 injection. The cavity wall average temperature also increases by 52°C (thus increasing from 1211°C in the allothermal mode to 1263°C in the hybrid mode).

To ascertain the functioning principle of the gasification process in the solar-combustion jet spouted bed, and to quantify the extent of spouting in the conical cavity, a representative 1.2 mm biomass particle stream was tracked all along its lifetime inside the reactor (Fig.6).

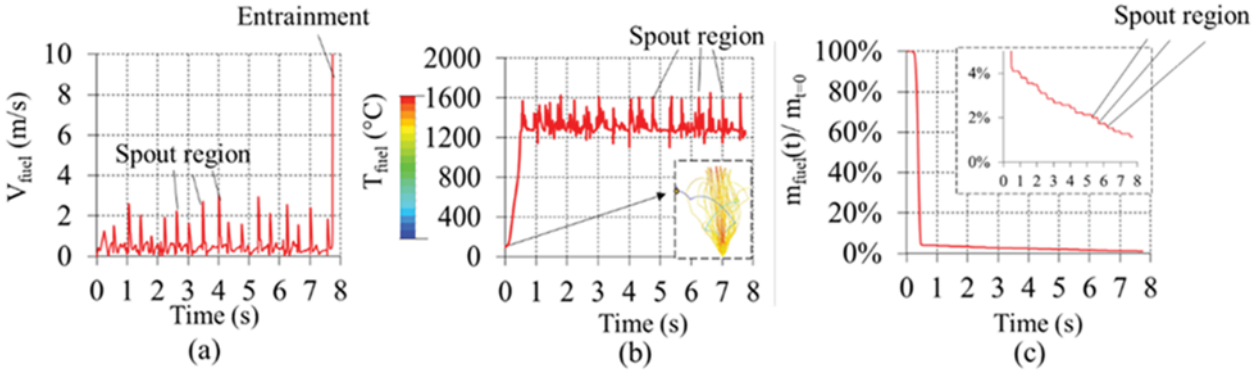

FIGURE 6. Biomass particle velocity, temperature and extent of particle conversion (for 1.2 mm initial particle size)

Fig.6a shows the biomass particle velocity as a function of its residence time in the cavity. It can be seen that the particle describes a number of cycles (from the spout to the annular region of the bed as evidenced by the successive velocity peaks) during which it pyrolyses and gasifies before being expelled from the reactor at the end of the stay. Fig.6b shows the particle temperature and the trajectory that it follows. It reveals that peak temperature values are reached when the particle moves over the spout region between the very hot combustion zone (flame zone) at the bottom area and the fountain zone near the radiation entrance where the particle/radiation entrance view factor is maximum. Fig.6c shows the conversion of the particle as a function of time. Two regions with two different slopes

can be observed. The sharp decrease in the particle mass during the first instants of injection is due to the fast pyrolysis of the particle. Char gasification subsequently occurs and constitutes the slowest step of the conversion process. For the allothermal operation, model predictions in terms of syngas composition were validated against previously obtained experimental data [18]. The simulated gas composition of the hybrid reactor was compared with the average calculated gas composition obtained in Run# 2 (between t=20min and t=38min) (Fig.7).

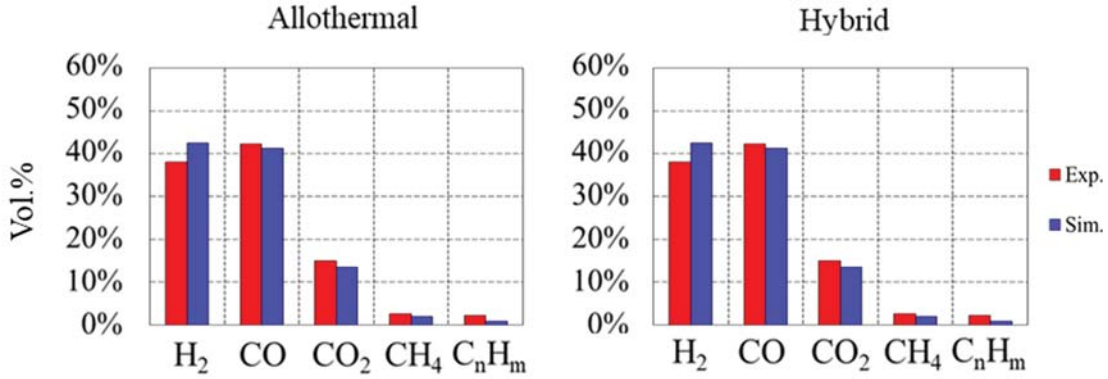

FIGURE 7. Simulated vs experimental molar gas composition

The predicted outlet gas composition in allothermal mode is in close agreement with the experimental measurements for the main gases including H_2, CO, CH_4, and CO_2 (relative discrepancy remains within a narrow range of 8% to 10%). Concerning the hybrid mode, the simulation also reproduces the global observed trends especially concerning the H_2 drop and the CO_2 sharp increase. However, it somewhat over predicts the H_2 yield at the expense of CH_4 and C_nH_m (including tars and light hydrocarbons). This can be due to an over predicted gas phase temperature in the central spout region related to the use of global kinetics for modelling gas phase chemistry. Further modelling of chemical reactions through detailed reaction mechanisms would be required to improve accuracy. It can be concluded that the 3D multiphase reactor model coupling mass, momentum and energy transport with both the reactive particulate phase (biomass) and the gas phase was fairly well validated by the experiments.

CONCLUSION

Hybrid solar/autothermal gasification was successfully simulated and tested in a spouted bed reactor. Oxy-combustion coupled to solar heating appeared to be a suitable option in order to control the reactor temperature. Experimental tests under real direct and indirect concentrated solar flux were conducted with the purpose of continuously gasifying a fixed amount of injected wood particles (1.2g/min). The switch to hybrid (solar/combustion) mode increased rapidly the reaction temperature in both heating configurations (direct and indirect) but lowered significantly the syngas yield (especially H_2). 3D simulations of the reactive gas-particle flow allowed a better understanding about the hybrid reactor operation. The same operating conditions were used in experiments to validate model predictions. O_2 injection should be used only when the available solar irradiation is insufficient to optimally convert the biomass feedstock. Furthermore, the observed decline of syngas quality (both heating value and H_2:CO ratio) due to hybridization can be an issue and needs to be mitigated to optimize process reliability and performance. This study represents the first successful attempt to control a hybrid thermochemical reactor under real solar irradiation and paves the way for continuous solar gasification processes.

ACKOWLEDGMENTS

This study was financially supported by ADEME (The French Environment and Energy Management Agency) and CEA (French Alternative Energy and Atomic Energy Commission). CNRS-PROMES is acknowledged for providing access to the solar installations.

REFERENCES

1. G.J.Nathan, M.Jafariana, B.B.Dally, W.L.Saw, P.J.Ashman, E.Hu, A.Steinfeld, Prog. Energy Combust. Sci., (2018) vol. 64, pp. 4–28.
2. A. Chinnici , G.J. Nathan, B.B. Dally, Applied Energy, (2018) vol. 224, pp. 426-437.
3. M. Puig-Arnavat, E.A. Tora, J.C. Bruno, A. Coronas, Sol. Energy (2013) vol. 97, pp. 67–84.
4. M. Sudiro and A. Bertucco, Energy Fuels, (2007) vol. 21, pp. 3668–3675.
5. T. Abe, N. Gokon, T. Izawa, T. Kodama, Energy Procedia (2015) vol. 69, pp. 1722–1730.
6. A. Z'Graggen, P. Haueter, D. Trommer, M. Romero, J.C. de Jesus, A. Steinfeld, Int. J. Hydrog. Energy, (2006) vol.31, pp. 797–811.
7. F. Müller, P. Pozˇivil, P.J. Van Eyk, A. Villarrazo, P. Haueter, Fuel, (2017) vol.193, pp. 432–443.
8. A. A. Kaniyal, P. J. van Eyk, G. J. Nathan, P. J. Ashman, and J. J. Pincus, Energy Fuels, (2013) vol. 27, pp. 3538–3555.
9. Xian Li, Ye Shen, Xiang Kan, Timothy Kurnia Hardiman, Yanjun Dai, Chi-Hwa Wang, Energy, (2017) vol. 142, pp.201-214.
10. A. Shirazi, A. Rahbari, C.-A. Asselineau, and J. Pye, Energy Convers. Manag., (2019) vol. 192, pp. 71–87.
11. A. P. Muroyama, I. Guscetti, G. L. Schieber, S. Haussener, and P. G. Loutzenhiser, Fuel, (2018) vol. 211, pp. 331–340.
12. L. Chen, thesis, Lyon 1, 2009.
13. J. Billaud, S. Valin, M. Peyrot, and S. Salvador, Fuel, (2016) vol. 166, pp. 166–178.
14. S. Septien, S. Valin, M. Peyrot, B. Spindler, and S. Salvador, Fuel, (2013) vol. 103, pp. 1080–1089.
15. J. Fermoso, C. Stevanov, B. Moghtaderi, B. Arias, C. Pevida, J. Anal. Appl. Pyrolysis, (2009) vol. 85, pp. 287–293.
16. C. Di Blasi, Prog. Energy Combust. Sci., (2009) vol. 35, pp. 121–140.
17. P. Nakod, Int. J. Chem. Ph. Sc, (2013) vol. 2.
18. Chuayboon, S., Abanades, S., Rodat, S.Chem. Eng. Process. - Process Intensif. (2018) vol. 125, pp. 253–265.